



Structure, microstructure, optical and magnetic properties of cobalt aluminate nanopowders obtained by sol-gel process

Youssef El Jabbar, Hind Lakhli, Rachida El Ouati, Lahcen Er-Rakho,
Sophie Guillemet, Bernard Durand

► To cite this version:

Youssef El Jabbar, Hind Lakhli, Rachida El Ouati, Lahcen Er-Rakho, Sophie Guillemet, et al.. Structure, microstructure, optical and magnetic properties of cobalt aluminate nanopowders obtained by sol-gel process. Journal of Non-Crystalline Solids, 2020, 542, pp.120115. 10.1016/j.jnoncrysol.2020.120115 . hal-02976870

HAL Id: hal-02976870

<https://hal.science/hal-02976870>

Submitted on 23 Oct 2020

HAL is a multi-disciplinary open access archive for the deposit and dissemination of scientific research documents, whether they are published or not. The documents may come from teaching and research institutions in France or abroad, or from public or private research centers.

L'archive ouverte pluridisciplinaire **HAL**, est destinée au dépôt et à la diffusion de documents scientifiques de niveau recherche, publiés ou non, émanant des établissements d'enseignement et de recherche français ou étrangers, des laboratoires publics ou privés.



Open Archive Toulouse Archive Ouverte



OATAO is an open access repository that collects the work of Toulouse researchers and makes it freely available over the web where possible

This is an author's version published in:

<http://oatao.univ-toulouse.fr/26799>

Official URL

DOI : <https://doi.org/10.1016/j.jnoncrysol.2020.120115>

To cite this version: El Jabbar, Youssef and Lakhlifi, Hind and El Ouatib, Rachida and Er-Rakho, Lahcen and Guillemet, Sophie  and Durand, Bernard  *Structure, microstructure, optical and magnetic properties of cobalt aluminate nanopowders obtained by sol-gel process.* (2020) Journal of Non-Crystalline Solids, 542. 120115. ISSN 0022-3093

Any correspondence concerning this service should be sent to the repository administrator: tech-oatao@listes-diff.inp-toulouse.fr

Structure, microstructure, optical and magnetic properties of cobalt aluminate nanopowders obtained by sol-gel process

Y. El Jabbar^{a,*}, H. Lakhli^a, R. El Ouati^b, L. Er-Rakho^a, S. Guillemet-Fritsch^b, B. Durand^b

^a Laboratoire de Physico-chimie des Matériaux Inorganiques, Faculté des sciences Aïn chock, Université Hassan II, Bp. 5366 Maarj, Casablanca, Morocco

^b Institut Carnot CIRIMAT, CNRS Université de Toulouse, 118 route de Narbonne, 31062 Toulouse Cedex 9, France

ABSTRACT

Keywords:
Nanoparticles
Morphology
Spinel
Amorphous
Blue
Complexing agent

The aim of this study was to determine the effect of different complexing agents and of the annealing temperature on the structural, morphological and optical properties of the synthesized precursors. Thus, cobalt aluminate nanoparticles were prepared by the sol-gel method using polyacrylic acid, glycine or citric acid as complexing agents. The synthesis performed at 500°C for 5 hours led to dark green powders composed of solid solutions denoted $\text{Co}^{2+}[\text{Al}_{2-x}^{3+}\text{Co}_{x-1}^{2+}]\text{O}_4$ and of amorphous alumina (39.8wt%). Calcination at temperatures above 900°C caused the powder colour to change from dark green to blue. A direct spinel structure $\text{Co}^{2+}[\text{Al}_{2-x}^{3+}]\text{O}_4$ is all the more achieved as the annealing temperature is high. The powder obtained using polyacrylic acid as the complexing agent at 900°C for 5 hours revealed the best morphology; it consisted of agglomerates of primary particles with a quasi-spherical shape and a size in the range 20–40 nm.

1. Introduction

Transition-metal aluminates with general formula MAl_2O_4 (M: Ni, Co, Fe) have attracted significant attention in recent decades because of their fundamental and applied interest. The excellent physical properties of these materials offer many possibilities for use in different fields, such as coatings, pigmentation and photocatalysis [1–6].

Cobalt aluminate spinel (CoAl_2O_4) is known for its blue colour and it is widely used as pigments for ceramics, paints, fibres and so on. Among its advantages, this compound presents high thermal and excellent chemical stability [7–10]. The spinel oxides powders are generally prepared by solid state reactions [11,12]. This method has the advantage of being simple and inexpensive, but it requires long thermal treatments at high temperatures ($T \sim 1300^\circ\text{C}$) [13,14]. Therefore, the resulting powders exhibit a low specific surface area, with morphologies that are most often heterogeneous. Recently, several research studies have focussed on the preparation of ultrafine CoAl_2O_4 powder for its use in the decoration of ceramics by ink-jet printers, which requires nanometric sizes to avoid clogging of the nozzles [15].

For the reasons described above, several soft-chemistry methods have been studied to prepare these materials, namely, the hydrothermal method [16], the co-precipitation route, the molten salt synthesis [17], the sol-gel process [18] and recently, the polymerisable complex method [19,20]. This last method provides nano-sized oxide powders

with high chemical and morphological homogeneities. This process uses a carboxylic acid as a chelating agent towards metal cations, which allows a mixed precursor to be obtained. The calcination of this latter leads to the formation of the mixed oxide at a relatively low temperature [21]. Several authors have shown that the morphological characteristics of powders synthesized by this process depend on the chemical nature of the chelating agent, the reaction pH, the calcination temperature and so on [22–26].

The aim of this work is to prepare nanosized CoAl_2O_4 powders using sol-gel synthesis with different complexing agents (polyacrylic acid, citric acid and glycine) at pH 7 and with different calcination temperatures. Then, the effect of the synthesis parameters on the structural, morphological, optical and magnetic properties of CoAl_2O_4 nanoparticles is studied. The use of this powder as a blue pigment is discussed.

2. Materials and methods

2.1. Synthesis

Cobalt nitrate $\text{Co}(\text{NO}_3)_2 \cdot 6\text{H}_2\text{O}$ (99.0%, Aldrich) and aluminum nitrate $\text{Al}(\text{NO}_3)_3 \cdot 9\text{H}_2\text{O}$ (99.0%, Aldrich) were dissolved in water at a molar ratio 1/2. Then an excess of one of the following complexing and gelling agents was added: polyacrylic acid (PAA) at a concentration of

* Corresponding author.

E-mail address: ysf.eljabbar@gmail.com (Y.E. Jabbar).

100 g L⁻¹, citric acid (CA) with molar ratio CA/cations = 3 or glycine (Gly) with a molar ratio Gly/nitrate = 2/3. After adjusting the pH to 7 by adding an ammonium hydroxide solution under constant stirring, the solution was evaporated at 80°C until obtaining a viscous gel, that was dried at 120°C for 24 hours (precursor noted PRO). Then the organic matter was removed by a precalcination at 300°C for 12 hours under air and cobalt aluminate samples noted PR1, PR2 and PR3 were obtained by annealing for 5 hours at respectively 500, 900 and 1100°C.

2.2. Characterization

The decomposition in air atmosphere of the pre-calcined powders (PRO) was investigated by differential thermal analysis and thermogravimetric analysis using a simultaneous DTA/TGA analyzer (DTA-TG-60H Shimadzu); the heating rate was set at 2.5°C/min. The X-ray diffraction patterns of the powders were recorded by means of a diffractometer equipped with a detector Lynx Eye (Bruker D8 Advance, $\lambda_{\text{CuK}\alpha}$ = 1.5406 Å). The infrared spectra were taken using FTIR spectrometer (IR affinity-15 Shimadzu). The morphology and size of the powders were examined with a field emission scanning electronic microscope (JEOL JSM 6700F) and the specific surface area were determined by the BET method (Micrometrics Flowsorb II 2300). The magnetic measurements were performed using a superconducting quantum interference magnetometer (SQUID, MPMS-XI). The absorbance spectra were determined by UV-Vis spectrophotometry (Perkin Elmer Lambda 35) and the colorimetric parameters (L*, a* and b*) were measured in the system (CIE) using a colorimeter (Chroma Meter CR-400/410, Konica Minolta).

3. Results and discussion

3.1. Thermal analysis

The thermal analysis curves of the PRO precursors prepared with different complexing and gelling agents and obtained after pyrolysis at 300°C for 12 hours are illustrated in Fig. 1. The TG curves of the PRO_{PAA} and PRO_{Gly} precursors (Figs. 1a and 1b) showed a total weight loss of about 15% and 12%, respectively, due to the elimination of the adsorbed water and the organic residues. The thermogram of the PRO_{CA} precursor presented a weight loss of about 23%, and the DTA curve showed a strong exothermic peak around 415°C (Fig. 1c). This could be attributed to the combustion of organic matter [27]. An additional slight endothermic inflection at 920°C was observed for the three precursors decomposition; this phenomenon might be due to the reduction of trivalent cobalt.

3.2. Powder X-ray diffraction analysis

The XRD patterns of the samples prepared with PAA, CA and Gly as complexing agents and heat treated at different temperatures are given in Fig. 2. Those of PRO_{PAA} and PRO_{Gly} showed some small peaks, indicating the beginning of crystallization, while the one of PRO_{CA} showed an amorphous phase. The annealing at 500°C/5h of PRO precursors with different complexing and gelling agents led to dark green powders PR1. The XRD patterns of these powders showed several peaks at 2θ values of 31.1°, 36.8°, 44.7°, 55.7°, 59.4°, 65.3°, 74.2° and 77.4°. These peaks could be indexed with space group Fd3m to (220), (311), (400), (422), (511), (440), (620) and (533) planes of a cubic unit cell. The Rietveld refinement pattern of the PR1 sample obtained with PAA as complexing agent is given in Fig. 3. The corresponding data (Table 1) showed that cobalt ions were located both in the tetrahedral 8a and octahedral 16d sites, whereas the aluminium ions predominantly occupied the octahedral 16d sites. This could indicate a partial oxidation of Co²⁺ in Co³⁺, giving the sample a greenish hue. Moreover, the structural properties (cell parameter, cell volume and density) deduced from the Rietveld refinement (Table 2) are intermediate between those

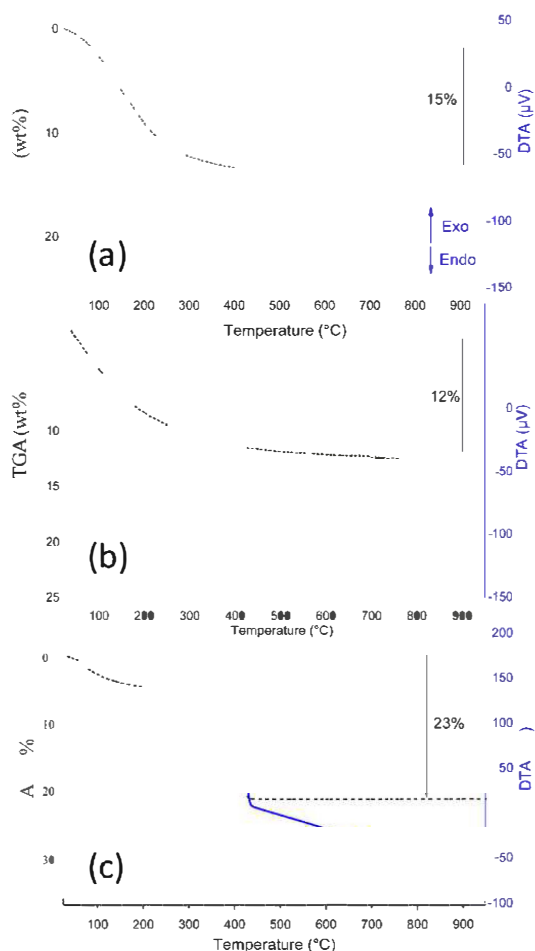


Fig. 1. Thermal analysis (TGA-DTA) curves of dried gel precalcined at 300°C for 12h PRO_{PAA} (a), PRO_{Gly} (b) and PRO_{AC} (c).

of the direct spinel phases Co²⁺[Co³⁺]₂O₄ and Co²⁺[Al³⁺]₂O₄. It is then concluded that the PR1 dark green powders are solid solutions between the two spinel phases, denoted Co²⁺[Al³⁺_{2(1-x)}Co³⁺_x]₂O₄.

In these PR1 powders, the unreacted aluminium is present, beside the crystallized spinel phase, under the form of amorphous alumina. In agreement with Yan et al [28], the internal standard method was involved to quantify the amorphous phase in the samples. This method consists in using an exact quantity of well-crystallized α-Al₂O₃ powder to be mixed and milled with the studied sample. The calculation of the percentage of amorphous phase present in a powder was done using the FullProf software by Rietveld refinement of diagram patterns. The percentages of the phases obtained by refinement were corrected with those of the prepared mixture. This allowed the rate of amorphous phase to be deduced. The content in amorphous alumina of the PR_{PAA} sample is about 39.8 wt%.

Whatever the nature of the complexing agent, blue powders PR2 and PR3 were obtained by annealing the PR1 powders at respectively 900°C/5h and 1100°C/5h. Their XRD patterns (Fig. 2) showed the same system of lines as the PR1 samples but they were narrower and became

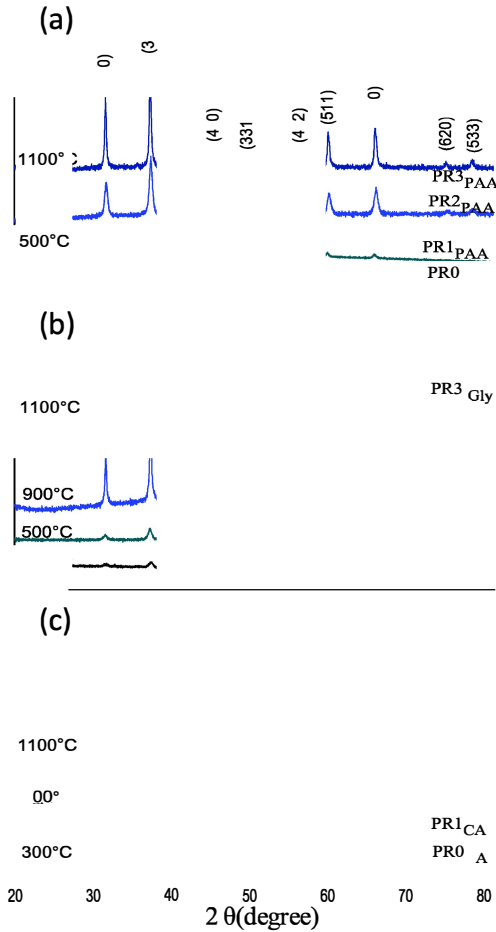


Fig. 2. X-ray powder diffraction patterns of PR0, PR1, PR2 and PR3 samples.

more intense, indicating higher crystallinity. All the diffraction peaks well matched with the standard JCPDS data for the direct spinel $\text{Co}^{2+}[\text{Al}_2^{3+}]_2\text{O}_4$ (JCPDS file n° 70-0753). The appearance of the reflection 331 at 49.3° (Figs. 2 and 3) is characteristic of the blue spinel compound $\text{Co}^{2+}[\text{Al}_2^{3+}]\text{O}_4$ [29]. The structural analysis by XRD revealed that no effect of the complexing agent was observed for the samples obtained at a annealing temperature equal or superior to 900°C . The structural refinement for PR2_{PAA} and PR3_{PAA} samples (Table 1) showed that the cobalt ions were located in tetrahedral sites and the aluminium ions occupied octahedral sites. This confirms a structure close to that of the direct spinel $\text{Co}^{2+}[\text{Al}_2^{3+}]\text{O}_4$. The structural properties (cell parameter, cell volume, density) also became closer to those of this spinel (Table 2). Simultaneously the amount of amorphous alumina decreased respectively to 8.3 and 2.9 wt%.

Consequently the transformation of the intermediate dark green solid solutions PR1 obtained at 500°C in blue spinel phases close to $\text{Co}^{2+}[\text{Al}_2^{3+}]\text{O}_4$ can be explained, in agreement with Pacewska et al [30], by the incorporation of amorphous alumina according to Eq. (1):

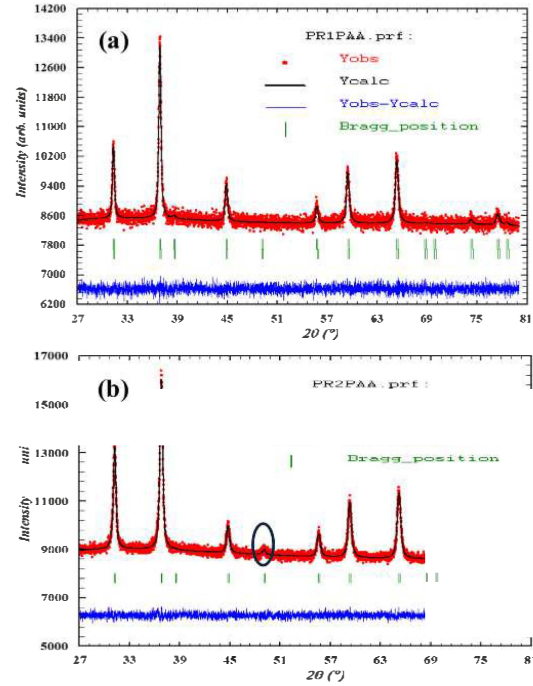
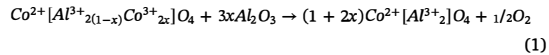


Fig. 3. Experimental, calculated and difference signals for PR1 (a) and PR2 (b) samples.

Table 1
Rietveld refinement for PR1_{PAA} , PR2_{PAA} and PR3_{PAA} samples.

Sample	Atom	Wyckoff Positions $X=y=z$	Occupancy	Biso	Refinement quality parameters
PR1 (500°C/5h)	Co	0.125	0.78	0.114(5)	$R_p=0.87\%$ $R_{wp}=1.09\%$ $\chi^2=1.03$
	Al	0.125	0.08	0.114(5)	
	Co	0.5	0.51	0.207(3)	
	Al	0.5	0.43	0.207(3)	
	O	0.262(4)	1	0.502(6)	
	Co	0.125	0.88	0.899(3)	
PR2 (900°C/5h)	Al	0.125	0.02	0.899(3)	$R_p=0.87\%$ $R_{wp}=1.08\%$ $\chi^2=1.05\%$
	Al	0.5	0.84	0.642(7)	
	Co	0.5	0.10	0.642(7)	
	O	0.263(3)	1	0.744(5)	
	Co	0.125	0.90	0.468(4)	
	Al	0.125	0.10	0.468(4)	
PR3 (1100°C/5h)	Al	0.5	0.92	0.314(3)	$R_p=0.95\%$ $R_{wp}=1.20\%$ $\chi^2=1.18\%$
	Co	0.5	0.06	0.314(3)	
	O	0.264(6)		0.268(5)	



The transformation is all the more complete as the annealing temperature is high. The mechanism of amorphous alumina insertion during the calcination of the gels is illustrated in Fig. 4.

3.3. FTIR spectroscopy analysis

The infrared spectra of the prepared samples are given in Fig. 5. The PR0_{PAA} and PR0_{Gly} spectra show two weak bands in the spectral range $500\text{--}700\text{ cm}^{-1}$. While in the PR0_{CA} spectrum, no IR band is observed.

Table 2

Structural properties and amorphous phase ratio for PR1, PR2 and PR3 sample obtained by Rietveld method refinements.

Structural properties	Co ₃ O ₄ JCPDS 76-1802	Samples PR1 _{PAA} (500°C/5h)	PR2 _{PAA} (900°C/5h)	PR3 _{PAA} (1100°C/5h)	CoAl ₂ O ₄ JCPDS 70-0753
Cell parameters (Å)	8.072	8.076(4)	8.092(4)	8.097(1)	8.095
Volume (Å ³)	525.95	526.68	529.71	530.85	530.46
Density (g/cm ³)	6.08	5.74	4.72	4.69	4.43
Amorphous phase ratio (Internal standard method)		39.8	8.3	2.9	

The PR1 spectrum shows two bands in the spectral range 500–700 cm⁻¹ whatever the nature of the complexing agent. These bands could be attributed to the Co²⁺ [Al³⁺_{2(1-x)}Co³⁺_{2x}]O₄ solid solution. The width of the peaks indicates the presence of amorphous phases in the sample [13]. When the thermal treatment raised-up 900°C (PR2 and PR3), a supplementary band appeared at 501 cm⁻¹ and the two other bands became more visible at 563 and 669 cm⁻¹. These three bands are attributable to the vibration modes of the CoAl₂O₄ phase [31]. These results are in good agreement with XRD analysis.

3.4. Magnetic measurement

The mixed and direct spinel structures were characterized using magnetic measurements. The PR1_{PAA} and PR2_{PAA} powders were analysed using a SQUID magnetometer in the temperature range 50–300K. Isothermal magnetization measurements (σ) as a function of the applied field (H) were performed at 50 and 300K. The evolutions of $\sigma=f(H)$ curves illustrated in Fig. 6a and b showed that the magnetization σ is a linear function of the applied field, according to the following equation:

$$\sigma = \chi \cdot H \quad (2)$$

χ : the magnetic susceptibility of the compound.

H: the applied field (Oe).

Therefore, the PR1_{PAA} and PR2_{PAA} compounds exhibited a paramagnetic behaviour at 50 and 300K. A small deviation of the slope of $\sigma=f(H)$ was observed between PR1_{PAA} and PR2_{PAA}; this indicated a significant influence of the calcination temperature on the magnetic properties of the samples studied.

Magnetic susceptibility measurements χ were made under a constant field of 10,000 Oe in the temperature range 50–300K, as presented in Fig. 7. The obtained curves evolutions were in good agreement with the Curie-Weiss law and could therefore be given by the following equation:

$$\chi = \frac{C}{T + \theta_p} \quad (3)$$

C: Curie constant.

T: Temperature (K).

θ_p : Paramagnetic Curie temperature (K).

Based on the linear evolution of the inverse molar magnetic susceptibility, the effective magnetic moment could be extracted for different samples. The value obtained for PR2_{PAA} was close to 4.65 μ_B . This value characterizes Co²⁺ in a tetrahedral site with a spin-orbit interaction (Lande g-factor [g]=2.4 and a spin [S]=3/2) [12]. This confirmed the Rietveld refinements, which presented a direct spinel structure for the PR2_{PAA} sample. However, the observed value for PR1 was 3.74 μ_B far from that of isolated Co²⁺ ($\mu_{eff} = 4.65 \mu_B$). This suggested that a mixture of Co²⁺ and Co³⁺ existed in this compound [32,33]. Table 3 shows the comparison of the experimental values of the effective magnetic moments with those theoretically obtained by applying the following equation [34]:

$$\mu_{eff}^2 = nx\mu_{eff}(Co_{Td}^{2+})^2 + 2ny\mu_{eff}(Co_{Oh}^{3+})^2 \quad (4)$$

n: percentage of the crystalline phase obtained by the internal standard method.

In Eq. (4), x and y are the fraction of cobalt Co²⁺ in tetrahedral sites (Td) and the fraction of Co³⁺ in octahedral sites (Oh), respectively. The theoretical values of $\mu_{eff}(Co_{Td}^{2+}) = 4.65 \mu_B$ and $\mu_{eff}(Co_{Oh}^{3+}) = 0 \mu_B$ (Co³⁺ was considered in low spin). The effective magnetic moments calculated by Eq. (4) were close to those obtained experimentally; and confirmed the results obtained by Rietveld refinement analysis.

3.5. Colour characterization

The heat treatment (500 ≤ T ≤ 1100°C) under air of the precursors

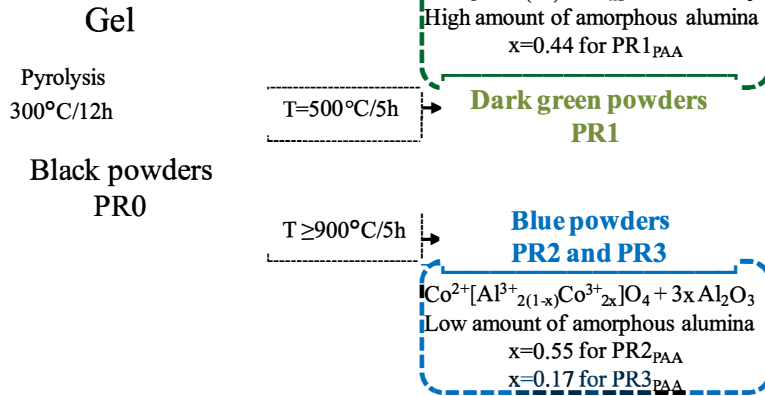


Fig. 4. Mechanism of alumina insertion.

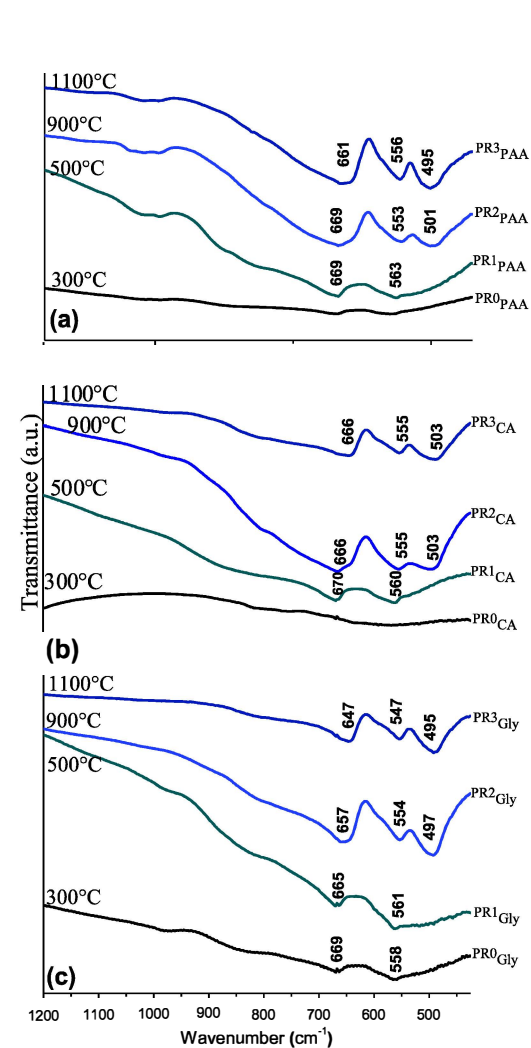


Fig. 5. FTIR spectra of PR0, PR1, PR2 and PR3 samples prepared by different complexing agents.

pre-calcined at 300°C for 12h (PR0 black) led to different shades of coloured powders. Indeed, the green colour was obtained at 500°C/5h (PR1) while the blue colour was observed from 900°C/5h (PR2 and PR3) (Fig. 8). The colorimetric and UV-Visible analyses were performed in order to correlate the optical properties with the chemical composition of the obtained powders. The PR1 powder obtained at 500°C had weak parameters a^* and b^* where the observed colour is of green shade. At temperatures above 900°C (PR2 and PR3), the parameter ($-b^*$) indicating the degree of blueing increased strongly so the blue shade was then observed. The colour shift from green to blue could be explained by the reduction of Co^{3+} to Co^{2+} with a change of coordination [35]. This blue color which represents CoAl_2O_4 compound was confirmed by three absorption bands in UV-Visible observed at 551, 590 and 628 nm (Fig. 9) which are due to the permissible spin

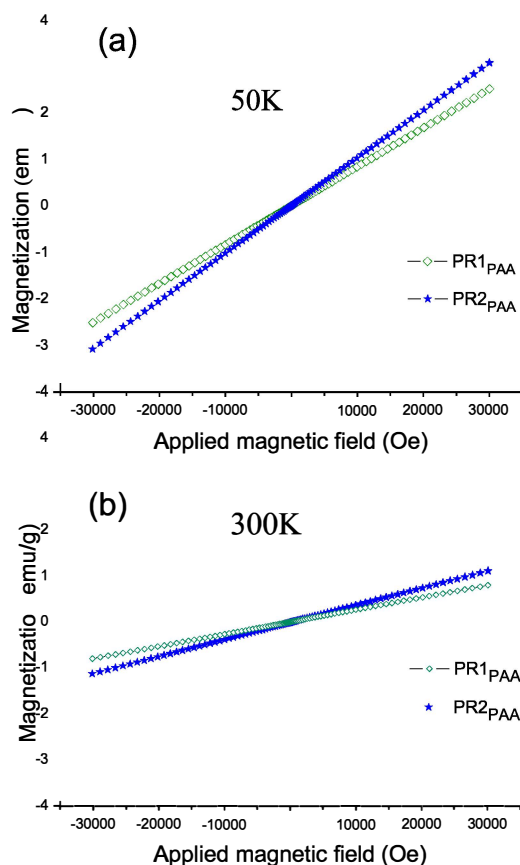


Fig. 6. Isothermal magnetization versus applied magnetic field for PR1 and PR2 samples.

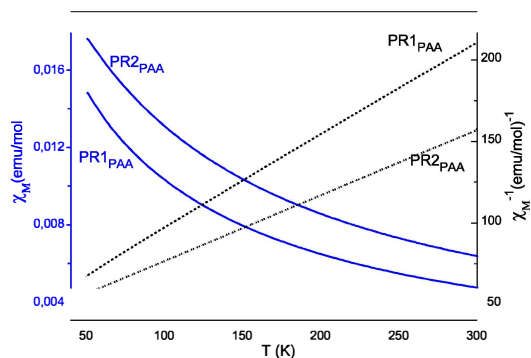


Fig. 7. Magnetic susceptibility for PR1 and PR2 samples.

Table 3
Effective magnetic moments of samples PR1_{PAA} and PR2_{PAA}.

Samples	$\mu_{\text{eff}}(\text{theoretical})(\mu_B)$	$\mu_{\text{eff}}(\text{experimental})(\mu_B)$
	3.59	3.74
	4.52	4.58

transitions of 3d electrons of Co^{2+} ions in tetrahedral coordination [4A2 (F) \rightarrow 4T1 (P)] which are responsible for the blue colouring [36].

3.6. Microstructure characterizations

The FE-SEM micrographs of the $\text{Co}^{2+}[\text{Al}_{2(1-x)}\text{Co}_{2x}^{3+}]\text{O}_4$ blue powders (PR2 and PR3) prepared with different complexing agents are presented in Fig. 10. The images of PR2_{PAA} (Fig. 10a) revealed ultrafine powders with quasi-spherical shapes and a size of 20–40 nm. In PR3_{PAA}, the particle sizes grew with increasing calcination temperatures, as shown in Fig. 10b. The powders, obtained at 900°C for 5 hours and synthesized using citric acid as the complexing agent (PR2_{CA}), showed agglomerates of variable shapes and the particle diameter was in the range 15–40 nm (Fig. 10c). The increase of the annealing temperature (1100°C for 5 hours) favoured the densification of the powder (PR3_{CA}), which indicated a pre-sintering. Grain growth was also observed (Fig. 10d). In contrast, in the powders obtained using glycine as the complexing agent (PR2_{Gly}), the powders were formed by porous agglomerates consisting of very fine particles that were difficult to individualize (Fig. 10e). The increasing of the annealing temperature created compact agglomerates, indicating an early pre-sintering (Fig. 10f). These powders had the particularity of being porous, which is due to the sudden departure of gases produced during the combustion of the precursors.

Surface area measurements (BET) were carried out for the different samples. As shown in Table 4, the specific surface area decreased with the annealing temperature and reached a high value (34 m²g^{−1}) for the PR2_{PAA} powders.

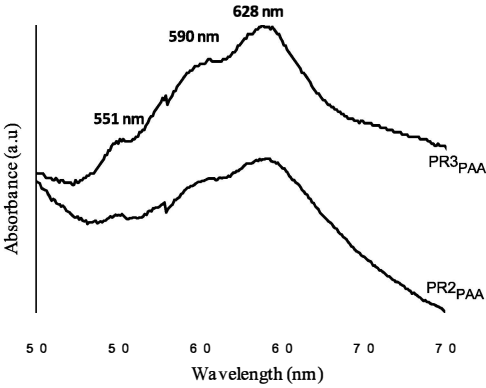


Fig. 9. PR2_{PAA} and PR3_{PAA} UV-Visible spectra.

4. Conclusion

Cobalt aluminates nano powders were prepared through sol-gel method. Further heat treatment performed at 500°C for 5 hours led to green powders. The composition was a mixed valence spinel structure denoted $\text{Co}^{2+}[\text{Al}_{2(1-x)}\text{Co}_{2x}^{3+}]\text{O}_4$ with a 39.8% Wt% amorphous phase. Calcinations at temperatures above 900°C created blue powders with a direct spinel structure (CoAl_2O_4). The colour shift from green to blue was explained by the reduction of Co^{3+} to Co^{2+} with a change of coordination. The influence of the complexing agent on the texture of the elaborated powders was remarkable. Indeed, the powder prepared using polyacrylic acid as the complexing agent and obtained at 900°C for 5 hours (PR2_{PAA}) shows homogenous morphology; it consists in agglomerates of primary particles of quasi-spherical shape with a size in the range 20–40 nm.

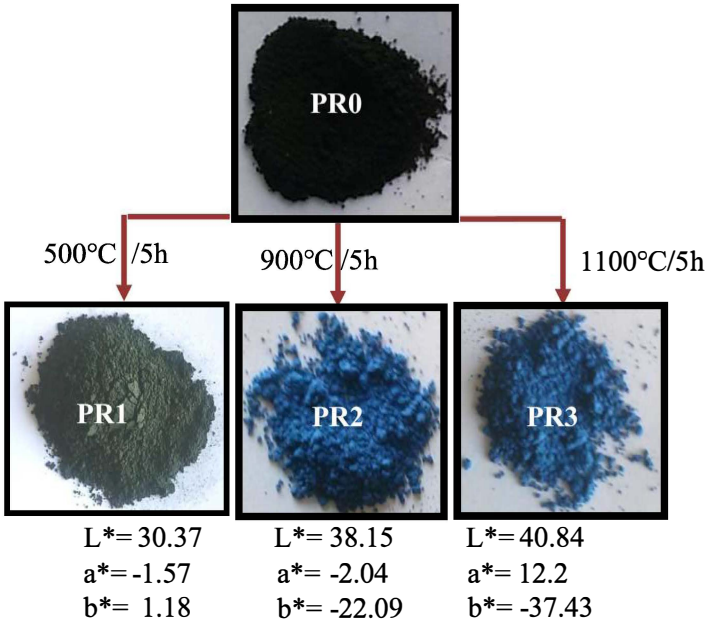


Fig. 8. L * a * b * Colourimetric parameters of powders prepared by PAA as complexing agent at pH = 7.

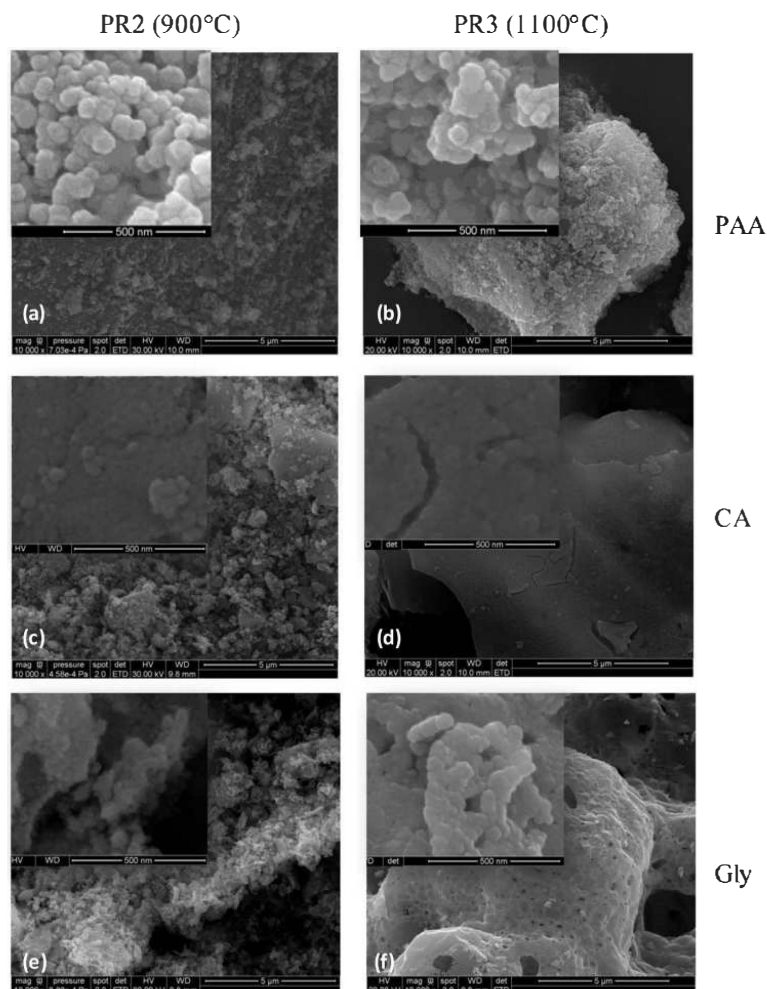


Fig. 10. SEM micrographs of samples obtained at 900°C (a,c,e) and 1100°C (b,d,f) with different complexing agents.

Table 4

BET surface area for PR2 and PR3 as a function of the complexing agent.

Sample/Complexing agent	Surface specific area (m ² /g)		
	PAA	Citric acid	Glycine
PR2	34.26	31.63	26.39
PR3	14.63	15.55	10.42

CRediT authorship contribution statement

Y. El Jabbar: Conceptualization, Writing - original draft. H. Lakhli: Software, Formal analysis. R. El Ouati: Supervision, Project administration, Validation. L. Er-Rakho: Methodology. S. Guillemet-Fritsch: Resources. B. Durand: Investigation, Visualization, Supervision, Data curation.

Declaration of Competing Interest

All authors declare no conflict of interests.

References

- [1] R.M. Bouck, A.M. Anderson, C. Prasad, M.E. Hagerman, M.K. Carroll, Cobalt-alumina sol gels: effects of heat treatment on structure and catalytic ability, *J. Non-Cryst. Solids* 453 (2016) 94–102, <https://doi.org/10.1016/j.jnoncrysol.2016.09.013>.
- [2] P.M.T. Cavalcante, M. Dondi, G. Guarini, M. Raimondo, G. Baldi, Colour performance of ceramic nano-pigments, *Dyes Pigments* 80 (2009) 226–232, <https://doi.org/10.1016/j.dyepig.2008.07.004>.
- [3] L.S. Lobo, A.R. Kumar, Structural and electrical properties of ZnCo₂O₄ spinel synthesized by sol-gel combustion method, *J. Non-Cryst. Solids* 505 (2019) 301–309, <https://doi.org/10.1016/j.jnoncrysol.2018.11.004>.
- [4] M. Maczka, M. Ptak, M. Kumatowska, J. Hanuza, Synthesis, phonon and optical properties of nanosized CoCr₂O₄, *Mater. Chem. Phys.* 138 (2013) 682–688, <https://doi.org/10.1016/j.matchemphys.2012.12.039>.
- [5] Y. Tong, H. Zhang, S. Wang, Z. Chen, B. Bian, Highly Dispersed re-doped CoAlO₄ nanopigments: synthesis and chromatic properties, *J. Nanomater* (2016) (2016) 1–7, <https://doi.org/10.1155/2016/4169673>.

- [6] Y. El Jabbar, M. ElHafdi, M. Benchikhi, R. El Ouati, L. Er-Rakho, A. Essadki, Photocatalytic degradation of navy blue textile dye by nanoscale cobalt aluminate prepared by polymeric precursor method, *Environ. Nanotechnol. Monit. Manag.* 12 (2019) 100259, <https://doi.org/10.1016/j.enmm.2019.100259>.
- [7] N.M. Deraz, M.M. Fouda, structural Synthesis, morphological properties of cobalt-aluminum nano-composite, *Int. J. Electrochem. Sci.* 8 (2013) 2756–2767.
- [8] J. Gilabert, M.P. Gómez-Tena, V. Sanz, S. Mestre, Effect of secondary thermal treatment on crystallinity of spinel-type $\text{Co}(\text{CrAl})_2\text{O}_4$ pigments synthesized by solution combustion route, *J. Non-Cryst. Solids* (2018), <https://doi.org/10.1016/j.jnoncrysol.2018.02.026>.
- [9] Y. Song, Y.L. Zheng, Y.F. Tang, H.B. Yang, Fabrication and stability of CoAl_2O_4 ceramic pigment for 3D printing, *Mater. Sci. Forum* 898 (2017) 1935–1939, <https://doi.org/10.4028/www.scientific.net/MSF.898.1935>.
- [10] Q. Wang, Q. Chang, Y. Wang, X. Wang, J. Zhou, Ultrafine CoAl_2O_4 ceramic pigment prepared by Pechini-sacrificial agent method, *Mater. Lett.* 173 (2016) 64–67, <https://doi.org/10.1016/j.matlet.2016.03.014>.
- [11] N. Srisawad, W. Chaitree, O. Mekasuwandumrong, P. Praserttham, J. Panpranot, Formation of CoAl_2O_4 nanoparticles via low-temperature solid-state reaction of fine gibbsite and cobalt precursor, *J. Nanomater.* 2012 (2012) 1–8, <https://doi.org/10.1155/2012/108369>.
- [12] B. Roy, A. Pandey, Q. Zhang, T.W. Heitmann, D. Vaknin, D.C. Johnston, Y. Furukawa, Experimental evidence of a collinear antiferromagnetic ordering in the frustrated CoAl_2O_4 spinel, *Phys. Rev. B* 88 (2013) 174415, <https://doi.org/10.1103/PhysRevB.88.174415>.
- [13] N. Ouahdi, S. Guillemet, J.J. Demai, B. Durand, L. Er Rakho, R. Moussa, A. Samdi, Investigation of the reactivity of AlCl_3 and CoCl_2 toward molten alkali-metal nitrates in order to synthesize CoAl_2O_4 , *Mater. Lett.* 59 (2005) 334–340, <https://doi.org/10.1016/j.matlet.2004.10.013>.
- [14] F. Yu, J. Yang, J. Ma, J. Du, Y. Zhou, Preparation of nanosized CoAl_2O_4 powders by sol-gel and sol-gel-hydrothermal methods, *J. Alloys Compd.* 468 (2009) 443–446, <https://doi.org/10.1016/j.jallcom.2008.01.018>.
- [15] Z. Pan, Y. Wang, H. Huang, Z. Ling, Y. Dai, S. Ke, Recent development on preparation of ceramic inks in ink-jet printing, *Ceram. Int.* 41 (2015) 12515–12528, <https://doi.org/10.1016/j.ceramint.2015.06.124>.
- [16] J.-H. Kim, B.-R. Son, D.-H. Yoon, K.-T. Hwang, H.-G. Noh, W.-S. Cho, U.-S. Kim, Characterization of blue CoAl_2O_4 nano-pigment synthesized by ultrasonic hydrothermal method, *Ceram. Int.* 38 (2012) 5707–5712, <https://doi.org/10.1016/j.ceramint.2012.04.015>.
- [17] N. Ouahdi, S. Guillemet, B. Durand, R. El Ouati, L. Er-Rakho, R. Moussa, A. Samdi, Synthesis of CoAl_2O_4 by double decomposition reaction between LiAlO_2 and molten KCoCl_3 , *J. Eur. Ceram. Soc.* 28 (2008) 1987–1994, <https://doi.org/10.1016/j.jeurceramsoc.2007.12.035>.
- [18] N. Bayal, P. Jeevanandam, Synthesis of metal aluminate nanoparticles by sol-gel method and studies on their reactivity, *J. Alloys Compd.* 516 (2012) 27–32, <https://doi.org/10.1016/j.jallcom.2011.11.080>.
- [19] M. Jafari, S.A. Hassanzadeh-Tabrizi, M. Ghahang, R. Pournajaf, Characterization of Ba^{2+} -added alumina/cobalt nanoceramic pigment prepared by polyacrylamide gel method, *Ceram. Int.* 40 (2014) 11877–11881, <https://doi.org/10.1016/j.ceramint.2014.04.022>.
- [20] M. Jafari, S.A. Hassanzadeh-Tabrizi, Preparation of CoAl_2O_4 nanoblu pigment via polyacrylamide gel method, *Powder Technol.* 266 (2014) 236–239, <https://doi.org/10.1016/j.powtec.2014.06.018>.
- [21] L. Gama, M.A. Ribeiro, B.S. Barros, R.H.A. Kiminami, I.T. Weber, A.C.F.M. Costa, Synthesis and characterization of the NiAl_2O_4 , CoAl_2O_4 and ZnAl_2O_4 spinels by the polymeric precursors method, *J. Alloys Compd.* 483 (2009) 453–455, <https://doi.org/10.1016/j.jallcom.2008.08.111>.
- [22] Y. El Jabbar, R. El Ouati, L. Er-Rakho, B. Durand, Influence of temperature and pH on the morphology and the color of the CoAl_2O_4 prepared by sol gel method, *J. Mater. Env. Sci.* 6 (2015) 3452–3456.
- [23] Y.F. Gomes, P.N. Medeiros, M.R.D. Bomio, I.M.G. Santos, C.A. Paskocimas, R.M. Nascimento, F.V. Motta, Optimizing the synthesis of cobalt aluminate pigment using fractional factorial design, *Ceram. Int.* 41 (2015) 699–706, <https://doi.org/10.1016/j.ceramint.2014.08.125>.
- [24] M.C.G. Merino, A.L. Estrella, M.E. Rodriguez, L. Acuña, M.S. Lassa, G.E. Lascala, P. Vázquez, Combustion syntheses of CoAl_2O_4 powders using different fuels, *Procedia Mater. Sci.* 8 (2015) 519–525, <https://doi.org/10.1016/j.mspro.2015.04.104>.
- [25] S. Salem, Effect of calcination temperature on colorant behavior of cobalt-aluminate nano-particles synthesized by combustion technique, *J. Ind. Eng. Chem.* 20 (2014) 818–823, <https://doi.org/10.1016/j.jiec.2013.06.011>.
- [26] L. Torkian, M. Daghighi, Effects of β -alanine on morphology and optical properties of CoAl_2O_4 nanopowders as a blue pigment, *Adv. Powder Technol.* 25 (2014) 739–744, <https://doi.org/10.1016/j.appt.2013.11.003>.
- [27] S.R. Prim, A. García, R. Galindo, S. Cerro, M. Llusar, M.V. Folgueras, G. Monrós, Pink ceramic pigments based on chromium doped $\text{M}(\text{Al}_{2-x}\text{Cr}_x)\text{O}_4$, $\text{M} = \text{Mg}$, Zn , normal spinel, *Ceram. Int.* 39 (2013) 6981–6989, <https://doi.org/10.1016/j.ceramint.2013.02.035>.
- [28] K. Yan, Y. Guo, Z. Ma, Z. Zhao, F. Cheng, Quantitative analysis of crystalline and amorphous phases in pulverized coal fly ash based on the Rietveld method, *J. Non-Cryst. Solids* 483 (2018) 37–42.
- [29] A.M. Wahba, N.G. Imam, M.B. Mohamed, Flower-like morphology of blue and greenish-gray $\text{ZnCo}_2\text{Al}_2\text{O}_4$ nanopigments, *J. Mol. Struct.* 1105 (2016) 61–69, <https://doi.org/10.1016/j.molstruc.2015.10.052>.
- [30] B. Pacewska, M. Keshr, Thermal transformations of aluminium nitrate hydrate, *Thermochim. Acta* 385 (2002) 73–80, [https://doi.org/10.1016/S0040-6031\(01\)00703-1](https://doi.org/10.1016/S0040-6031(01)00703-1).
- [31] X. Duan, M. Pan, F. Yu, D. Yuan, Synthesis, structure and optical properties of CoAl_2O_4 spinel nanocrystals, *J. Alloys Compd.* 509 (2011) 1079–1083, <https://doi.org/10.1016/j.jallcom.2010.09.199>.
- [32] M. Gabrovska, n. Stanica, d. Crisan, d. Nikolova, I. Bilyarska, M. Crisan, R. Edrevakardjieva, Co-Al layered double hydroxides as precursors of ceramic pigment CoAl_2O_4 . Part II: magnetic and tint properties, *Rev. Roum. Chim.* 59 (2014) 451–455.
- [33] L. Markov, K. Petrov, V. Petrov, On the thermal decomposition of some cobalt hydroxide nitrates, *Thermochim. Acta* 106 (1986) 283–292, [https://doi.org/10.1016/0040-6031\(86\)85140-1](https://doi.org/10.1016/0040-6031(86)85140-1).
- [34] M. Taguchi, T. Nakane, K. Hashi, S. Ohki, T. Shimizu, Y. Sakka, A. Matsushita, H. Abe, T. Funazukuri, T. Naka, Reaction temperature variations on the crystallographic state of spinel cobalt aluminate, *Dalton Trans.* 42 (2013) 7167, <https://doi.org/10.1039/c3dt32828g>.
- [35] S. Kurajica, J. Popović, E. Tkalčec, B. Gržeta, V. Mandić, The effect of annealing temperature on the structure and optical properties of sol-gel derived nanocrystalline cobalt aluminate spinel, *Mater. Chem. Phys.* 135 (2012) 587–593, <https://doi.org/10.1016/j.matchemphys.2012.05.030>.
- [36] I.S. Ahmed, A simple route to synthesis and characterization of CoAl_2O_4 nanocrystalline via combustion method using egg white (ovalbumine) as a new fuel, *Mater. Res. Bull.* 46 (2011) 2548–2553, <https://doi.org/10.1016/j.materresbull.2011.08.005>.